Physical Chemistry Chemical Physics

ARTICLE

Chromophores of chromophores: A bottom-up Hückel picture of the excited states of photoactive proteins

Received 00th January 20xx,
Accepted 00th January 20xx

DOI: 10.1039/x0xx00000x

www.rsc.org/

Cate S. Anstöter, Charlie R. Dean and Jan R. R. Verlet*

Many photoactive proteins contain chromophores based on para-substituted phenolate anions which are an essential component of their electronic structure. Here, we present a reductionist approach to gain fundamental insight into the evolution of electronic structure as the chromophore increases in complexity from phenolate to that in GFP. Using frequency- and angle-resolved photoelectron spectroscopy, in combination with electronic structure theory, the onset of excited states that are responsible for the characteristic spectroscopic features in biochromophores are determined. A comprehensive, yet intuitive picture of the effect of phenolate functionalisation is developed based on simple Hückel theory. Specifically, the first two bright excited states can be constructed from a linear combination of molecular orbitals localised on the phenolate and para-substituent groups. This essential interaction is first observed for *p*-vinyl-phenolate. This bottom-up approach offers a readily accessible framework for the design of photoactive chromophores.

Introduction

At the core of most photoactive proteins is a small organic chromophore that acts as a light activated switch for the protein's function. Many of these natural chromophores contain the phenolate anion, Ph^- (Figure 1). In the green fluorescent protein (GFP), the chromophore is often taken to be the deprotonated *p*-hydroxybenzylidene-2,3-dimethylimidazolinone ($HBDI^-$, Figure 1), which is hindered from undergoing isomerisation in the protein and consequently fluoresces with a very high quantum yield.[1,2] In the photoactive yellow protein (PYP), the chromophore is often taken to be deprotonated *p*-coumaric acid (CA^-, Figure 1), which undergoes a trans-cis isomerisation upon near UV-excitation and serves as a mechanical switch to initiate the protein's response.[3,4] The commonality of phenolates in many photoactive proteins arises from the biosynthetic pathways of chromophores that often involve tyrosine. The photophysics of photoactive protein chromophores has attracted much attention because of their underpinning role in the initial protein response to light.[5–7] Gas-phase spectroscopy has been particularly valuable as it provides an unperturbed view of the excited states of the chromophores and of their dynamics.[8–12] Additionally, the gas-phase environment is tractable by high-level electronic structure theory,[13–16] which when combined with experiment, provides a detailed understanding of the excited state dynamics. However, the reliance on very high level computational methods can mask some of the simple physical principles that are the foundation of the overall electronic structure of the chromophores. Such principles are central to the logical development of new light-activated proteins or macromolecules, and to understanding the natural selection based on nature's basic building blocks such as the amino acids. Here, we use gas-phase photoelectron imaging of the phenolate chromophores of $HBDI^-$ and CA^-. Based on our results, we provide a simple bottom-up picture of their bright excited states using Hückel theory together with electronic structure calculations. Specifically, we show that a simple linear combination of molecular orbitals (MO) gives rise to the characteristic spectroscopic features of these photoactive chromophores.

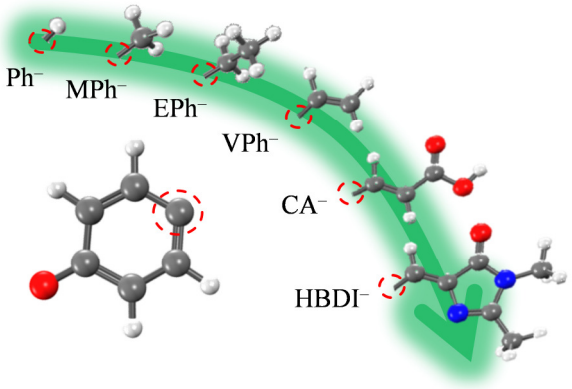

Figure 1: Schematic showing structures of chemically substituted para-phenolate chromophores with increasing complexity.

Department of Chemistry, Durham University, Durham, DH1 3LE, UK.
Email: j.r.r.verlet@durham.ac.uk

Electronic Supplementary Information (ESI) available: Experimental and computational energetics; Frequency-resolved photoelectron spectra of MPh^-; Anisotropy across two direct detachment channels; Excited states of MPh^- and EPh^-. See DOI: 10.1039/x0xx00000x

There is a wealth of experimental and computational studies on the photophysics of photoactive proteins and, specifically, their chromophores.[12,17–32] These have largely focussed on the first singlet excited (S_1) state of the chromophores, because this is generally the excited state that is the most relevant to the biological function of the protein. For example, the pioneering work by Andersen and co-workers showed that the absorption spectrum of $HDBI^-$ has a very similar appearance in vacuum as it does in the protein environment. The S_1 state of $HDBI^-$ has been the focus of a large number of gas-phase studies.[13,19,31,33–37] A very insightful picture of the electronic structure of the S_1 state was provided by Bravaya *et al*., who rationalised the energetic shifts in different coloured photoactive proteins using a 3-centre allyl radical in a simple Hückel framework and a particle in the box model.[38]

More recently, experimental and computational work has been directed to the higher-lying excited states in the UV spectral region. These are believed to be important in the photooxidation of the photoactive proteins. For example, in GFP a second optically bright state of $HBDI^-$, S_3, has been observed by action spectroscopy.[19] Photoelectron spectroscopic measurements with complementary computational studies suggest that the S_3 state leads to electron ejection from the protein to form hydrated electrons.[13] More generally, frequency-resolved photoelectron spectroscopy has provided valuable insight into the dynamics of resonances in the isolated chromophores, including $HBDI^-$.[13,39] High-level electronic structure calculations show that the S_3 resonance is formed by promotion of an electron from the highest occupied molecular orbital (HOMO) to an unoccupied π* MO localised almost exclusively on the phenolate chromophore. In a similar vein to the interpretation of the S_1 state, Bochenkova *et al*. viewed the MOs for the ground and excited electronic states using a cartoon Hückel picture to sketch the nature of transitions.[19] While high-level calculations allow quantitative analysis of experimental data, the simple models based on Hückel theory allow qualitative analysis that provides deep insight into the nature of electronic states, which is critical in the rational design of new photoactive proteins and macromolecules. This is particularly so from a synthetic chemist's perspective who may not have the highly specialised skills required to perform high-level electronic structure calculations. In this study, we generalise and validate a Hückel picture using a bottom-up approach. We show that the first two bright states of photoactive proteins arise from interaction of two chromophore moieties and that the phenolate chromophore is essential to describing the UV response of photoactive chromophores.

Methodology

Experimental

The experiment has been described in detail elsewhere.[40,41] Briefly, electrospray ionisation was used to produce deprotonated anions from ~1 mM solutions of phenol, *p*-methyl-phenol or *p*-ethyl-phenol in methanol. These phenolates (Ph^-, MPh^- and EPh^-, respectively) were introduced to the first of several vacuum regions by a transfer capillary before progressing along a series of ring-electrode ion guides. The anions were pulsed into a collinear Wiley-McLaren time-of-flight mass spectrometer[42] by an ion trap at the end of the ion guides. Mass-selected ion packets were then irradiated by a tunable ~6 ns laser pulse from a Nd:YAG pumped optical parametric oscillator (Continuum Surelite II-10, Horizon I), and photoelectrons produced were imaged using a velocity-map-imaging assembly.[43,44] The photoelectron spectrum and photoelectron angular distributions (PADs) were extracted from raw photoelectron images using the Polar Onion Peeling algorithm.[45] Photoelectron spectra were calibrated using the known atomic spectrum of I^- and have an experimental resolution of ~5%. The photoelectron spectra for $HBDI^-$ is reproduced from a previous study using the same experimental method.[33] As detailed in previous work,[46] *p*-vinyl-phenolate, VPh^-, was produced from CA^- that underwent collisional-induced dissociation to lose CO_2 in the ion guide. The anionic fragment was then mass-selected in the time-of-flight mass spectrometer before being irradiated to perform photoelectron imaging.

Computational

Hückel theory calculations were performed using the HuLiS calculator.[47,48] Additional electronic structure calculations of the ground and excited states of the deprotonated anions and corresponding neutral radicals were carried out using the QChem 4.4 package.[49] Initial density functional (DFT) calculations optimized the geometries of the ground states of neutral and anions. These geometries were confirmed to be energetic minima by vibrational frequency analysis. Time-dependent (TD) DFT calculations, with the Tamm-Dancoff approximation,[50] confirmed the character and energetics of the excited states of the neutral accessed experimentally. The results of these calculations are presented in the Electronic Supplementary Information (ESI) and used the B3LYP functional[51–54] and the aug-cc-pVDZ Dunning basis set.[55] Further calculations qualitatively explored changes to the character of the bright excited states of a series of para-substituted phenolates from phenolate to *p*-hydroxybenzylideneimidasolinone (HBI^-), as shown in Figure 1. These calculations were done using the B3LYP functional and the cc-pVDZ basis set, to exclude diffuse continuum states and simplify analysis of the molecular orbitals. This deliberately low level of theory was employed to allow qualitative comparison of MOs and their relative weightings to excited states with the results of the HuLiS calculator.

To model the angle-resolved data, all anions were optimized using coupled cluster singles and doubles (CCSD) method, with the same basis set as before. Using these optimized geometries the Dyson orbitals were calculated through implementation of the equation-of-motion CCSD (EOM-CCSD) formalism.[56,57] Further detail on the Dyson orbitals used to model the D_0 and D_1 direct detachment channels accessed experimentally can be found in previous

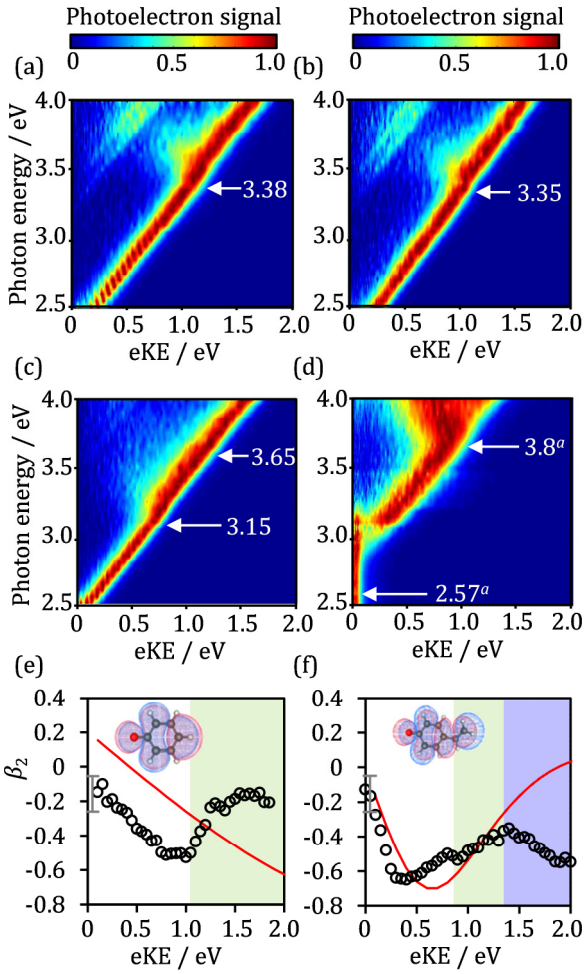

Figure 2: Frequency-resolved photoelectron spectra of (a) Ph^-, (b) EPh^-, (c) VPh^-, and (d) $HBDI^-$ (taken from ref 33) are shown. All photoelectron spectra are normalised to a unit maximum. The horizontal arrows indicate the onsets of resonances in eV. For $HBDI^-$, these are taken from ref 19. Anisotropy parameters (β_2) for (e) Ph^- and (f) VPh^- as a function of electron kinetic energy (eKE). Open circles and solid lines are experimentally and computationally determined β_2(eKE), respectively. Shaded eKE regions indicate resonance dynamics that change β_2 from the calculated ones. The parameters of the resonances are taken from the indicated experimental energies at which resonances are encountered shown in (a) and (c), for (e) and (f), respectively. The Dyson orbitals used to model the anisotropy computationally are inset.

work.[46] Finally, the PADs for the two direct detachment channels were calculated using the ezDyson program (version 3.2) developed by Krylov and co-workers.[58]

Results

The frequency-resolved photoelectron spectra for Ph^-, EPh^-, VPh^- and $HBDI^-$ are summarized as 3D false-colour plots in Figure 2(a)-(d), respectively. MPh^- is presented in the Figure ESI1 for completeness. To emphasize spectral changes as a function of photon excitation energy, *hv*, the photoelectron spectra have been normalised to a maximum intensity of one. At all *hv*, the photoelectron spectra are dominated by a feature with an electron kinetic energy (eKE) that increases linearly with increasing photon energy. This direct detachment channel corresponds to electron loss from the ground singlet state of the anion to form the ground doublet state of the corresponding neutral species, $S_0 + h\nu \rightarrow D_0 + e^-$. A second direct detachment feature for Ph^-, MPh^- and EPh^-, with an onset at *hv* ~ 3.2 eV, corresponds to the $S_0 + h\nu \rightarrow D_1 + e^-$ direct detachment channel. This channel is also seen for VPh^-, albeit relatively weaker and shifted to *hv* ~ 3.5 eV. It is not observable in $HBDI^-$.

In addition to the direct detachment features, spectral broadening is observed for all the anions, where photoelectron signal is observed at lower eKE than the direct detachment peak. Such shifts have been observed in the photoelectron spectra of many anionic species,[39,41,59–62] including several bio-chromophore derivatives based on phenolate.[8,13,22,33,36,63] The shift towards lower eKE arises from the excitation of an electronic resonance of the anion. This resonance can undergo nuclear motion which leads to changing Franck-Condon factors with the final neutral states to which it autodetaches. The spectral features are broadly similar for all the phenolates including $HBDI^-$, suggesting that a common motif is responsible for the observed dynamics. However, the onset and width of the resonance features can be seen to change most significantly between Ph^- and EPh^- to VPh^- and $HBDI^-$. Additionally, the cross-section of excitation to the resonance appears to be larger for the latter two as evidenced by the larger proportion of photoelectrons lost from the autodetachment channel than from the direct channel leaving the neutral in the D_1 state.

The experimental data allows key properties of the phenolate derivatives to be determined. This includes the vertical detachment energy (VDE) and adiabatic detachment energy (ADE), as well as the D_0-D_1 gap and the onset of the resonances (tabulated in ESI1). The resonance onsets were determined in two ways. They can be identified by the *hv* at which the indirect autodetachment signal can be observed (see Figure 2(a) – (d)). They can also be determined from sudden changes in PADs as a function of *hv*. Figure 2(e) and (f) show the experimentally determined anisotropy parameters (β_2) for Ph^- and VPh^-, respectively. The experimental β_2 parameter as a function of eKE were computed and their functionality followed the experimental values up to an eKE where a resonance can be accessed. Note that, although we recently showed that such an approach yields almost quantitative agreement,[41,46] the PADs appear to have a constant discrepancy for Ph^-, although the trend is correct. The Dyson orbital approach fails to capture autodetachment from resonance leading to PADs rapid deviations from calculated behaviour.[41,64] This has recently been observed in AgF^- and CuF^-, where qualitative arguments were used to account for the change in anisotropy for autodetachment from resonances.[65] Examples of similar behaviour for the present systems are shown in Figure 2(e) and (f) for Ph^- and VPh^-, respectively. There are two regions that show discontinuities for VPh^-, suggesting that there are two resonances present. The onset of the resonance derived from the photoelectron spectra and the PADs agree remarkably well with each other, providing confidence of the assignment, although we note that

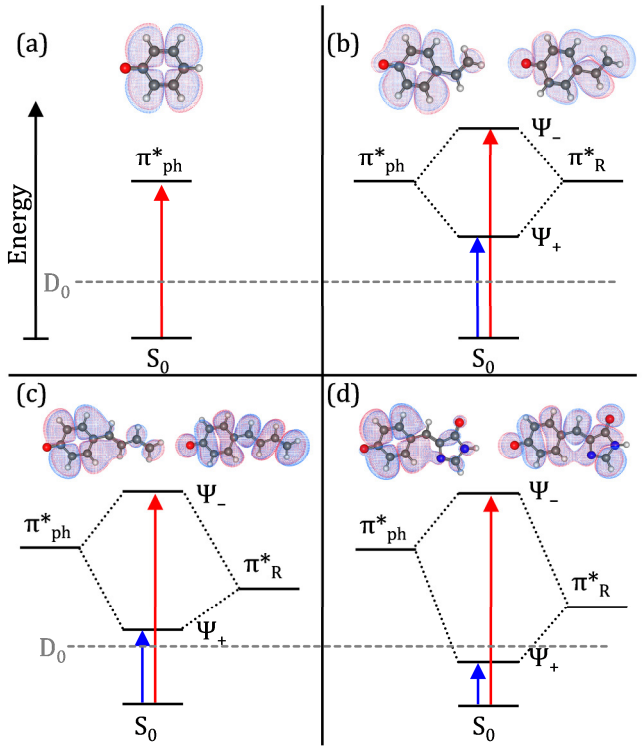

Figure 3: Relevant molecular orbitals (MOs) and schematic MO diagram of excited states of (a) Ph^-, (b) VPh^-, (c) BPh^-, and (d) $HBDI^-$. The π^*_{Ph} MO (left) produces a linear combination with the π^*_R MO (right) to produce the excited state structure of the chromophores. The neutral state, D_0, is also indicated.

there is no clear indication of the second resonance for VPh^-, except for the much greater range over which spectral broadening occurs in this anion. The onsets of observed resonances have been included in Figure 2(a) – (d) as horizontal arrows. Those for $HBDI^-$ are taken from the action spectrum of the Andersen group and agree with the values determined from the frequency-resolved photoelectron spectra in Figure 2(d).

In addition to ground state calculations, excited state calculations were performed. While the absolute energies are in poor agreement, the relative energies and patterns of states are expected to be less prone to large errors and these are used to provide a basis for the interpretation of the experimental data. The first bright resonance in Ph^-, MPh^- and EPh^- was calculated to be independent of substituent (see Figure ESI3), in agreement with experimental observations. This resonance corresponded to the promotion of an electron from the HOMOto an unoccupied antibonding MO localised on the phenol ring, π_{Ph}^*. The relevant orbital calculated by DFT for Ph^- is shown in Figure 3(a) and those for MPh^- and EPh^- are in the Figure ESI3. Autodetachment from the resonance correlates with a one-electron process, in which loss of the electron from the π_{Ph}^* orbital produces the D_0 ground neutral state. The resonance is therefore of shape character.[39] According to our calculations, for VPh^- there are two bright excited states. Both have mixed character with a combination of a similar π_{Ph}^* orbital as well as an unoccupied MO, π_R^* on the vinyl unit. This π_R^* orbital has the appearance of the π^*

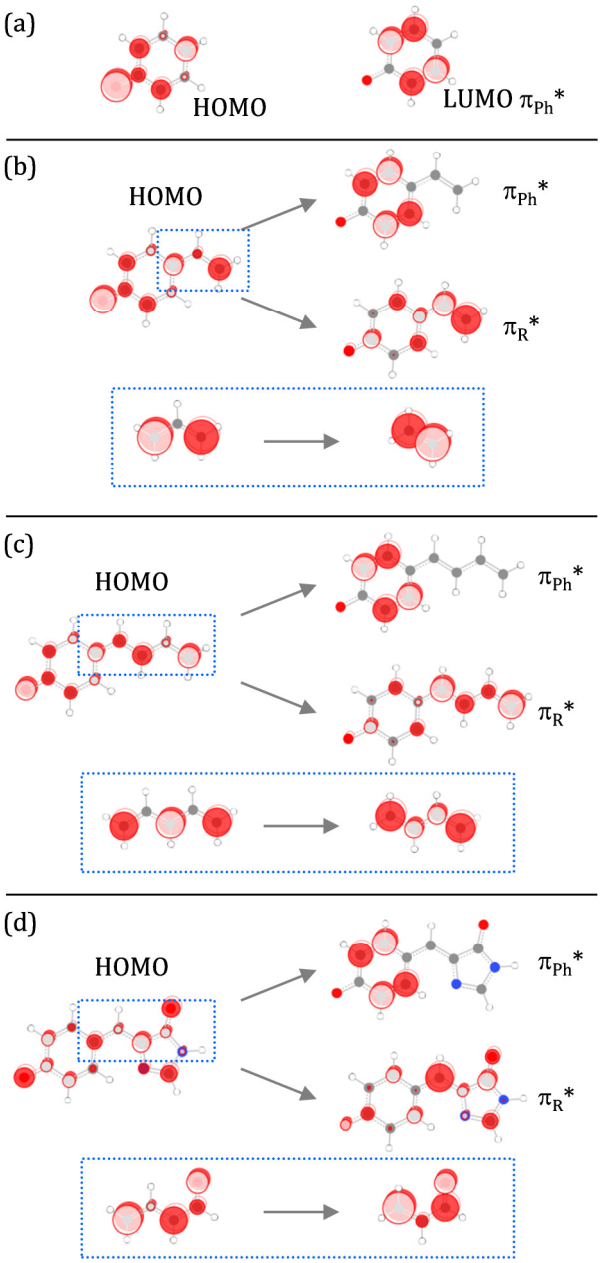

Figure 4: Highest occupied Hückel molecular orbital (HOMO) and lowest unoccupied molecular orbital (LUMO) and π^*_{Ph} and π^*_R MOs of (a) Ph^-, (b) VPh^-, (c) BPh^-, and (d) HBI^-. Marked insets in (b) – (d) show the chromophoric MOs involved in the HOMO → LUMO transition.

MO of ethene, as shown in Figure 3(b). The weights according to TD-DFT of the two excited states in terms of these orbitals are: $\Psi_+ = 0.60\ \pi_{Ph}^* + 0.76\ \pi_R^*$ and $\Psi_- = 0.75\ \pi_{Ph}^* - 0.58\ \pi_R^*$, where Ψ_+ is lower in energy than Ψ_-. The presence of two resonances in VPh^- accounts for the large width observed for the resonance autodetachment seen in Figure 2(c) and the changes noted in the PADs in Figure 2(f).

Discussion

A Hückel interpretation of excited states

The frequency resolved photoelectron spectra for Ph^-, MPh^- and EPh^- are essentially identical, which allows us to conclude that the addition of an alkyl group (R) at the para position of the phenolate does not affect the π_{Ph}* resonance energies, nor does it appear to affect the autodetachment dynamics from this resonance. This can be justified in a Hückel framework as the π_{Ph}* orbital has no electron density on the oxygen or the para-carbon atom which binds to the R group. Hence, the π_{Ph}* orbital essentially corresponds to a π* orbital of benzene with a Hückel energy of $\varepsilon = \alpha - \beta$. As it is a localised excitation, there is also no reason to expect the dynamics to differ as R changes. However, in the case of VPh^- and $HBDI^-$, the R group does perturb the excited state structure. The main difference in these cases is that the R group has its own π-system that is conjugated to the phenolate.

If the R group's π electron system is conjugated with the phenolate, then the HOMO becomes delocalised over the entire molecule. For VPh^- the HOMO calculated using DFT is shown in Figure 3(b), while Figure 4(b) shows the results from a simple Hückel calculation. Both calculations show the delocalised π electron nature of the HOMO. However, inspection of the Hückel HOMO allows us to approximate it as a combination of the HOMO of the phenolate (shown in Figure 4(a)) and the allyl radical (highlighted region in Figure 4(b)) with the para-carbon providing a common contribution. We now consider the unoccupied MOs of VPh^- within the Hückel framework.

The lowest-lying unoccupied MO has the appearance of the ethene antibonding orbital, π_R*, as shown in Figure 4(b).‡ The second unoccupied MO is the LUMO of phenolate, π_{Ph}*, which is localised because of the very small coefficients (i.e. almost a node) at the para-carbon. Assuming that π_R* can be approximated as the ethene π* MO, then the Hückel energies of the π_{Ph}* and π_R* are degenerate with an energy of $\varepsilon = \alpha - \beta$. We can now construct a simple MO diagram involving these π_{Ph}* and π_R* orbitals, as shown in Figure 3(b). A linear combination of π_{Ph}* and π_R* MOs will lead to two new MOs: $\Psi_\pm = 0.71\pi_{Ph}^* \pm 0.71\pi_R^*$. This is in very good agreement with the TD-DFT calculations that yield $\Psi_+ = 0.60\pi_{Ph}^* + 0.76\pi_R^*$ and $\Psi_- = 0.75\pi_{Ph}^* - 0.58\pi_R^*$. The Ψ_+ MO is reduced in energy compared to Ph^-, MPh^- and EPh^-, in good agreement with the results shown in Figure 2. The Ψ_- solution is expected to increase in energy by a similar amount relative to the π_{Ph}* MO because of the nearly equal contribution of both MOs to wavefunctions. The separation of the two states is 0.5 eV from the experiment (Figure 2(c)), suggesting a shift of ~0.25 eV of Ψ_+ and Ψ_-, relative to their non-interacting MOs.

In addition to the spectral agreement, the above analysis agrees with the observed experimental changes in the resonance dynamics. The autodetachment dynamics that can be ascertained from the spectral broadening appears to be similar for the two resonances of VPh^-. This is in line with the fact that both have equal contributions from the π_{Ph}* MO which is of shape character and is responsible for the autodetachment as seen in Figure 2(a) and (b). Additionally, the transition strength appears to have increased for both Ψ_+ and Ψ_- in VPh^- compared to the excitation to the pure π_{Ph}* state in Ph^-. This can be rationalised by the $^1\pi\pi^*$ character in the excitation that comes about from the bright n(allyl) → π*(ethene) transition (see inset of Figure 4(b)).

It is also noted that energy gap between the HOMO and the π_{Ph}* MO is not drastically affected by para-substitution. This can be appreciated by inspection of Figure 3(b), which shows that the HOMO of VPh^- is qualitatively the same as that of Ph^- because the conjugated R group is non-bonded due to a central allyl node. In fact, this argument essentially remains true for all phenolates discussed here.

We now extend this Hückel analysis to larger conjugated molecules. We begin by considering 1,3-butadienylphenolate (BPh^-), Figure 3(c) and 4(c). For this molecule, R can be approximated as pentadiene bound to phenolate with the common para-carbon (see Figure 4(c) inset). The unoccupied MOs can be considered in a similar spirit as above. The π_{Ph}* MO is the same as that of VPh^- and Ph^-. The π_R* MO can be viewed as the first π* MO of butadiene (see Figure 4(c) inset), which has a Hückel energy $\varepsilon = \alpha - 0.62\beta$. The reduction of the orbital energy of π_R* relative to π_{Ph}* means that their linear combination of π_R* with π_{Ph}* results in a lower energy of Ψ_+, while Ψ_- will remain at approximately the same energy as Ψ_- in VPh^-. The linear combination of MO will lead to Ψ_+ and Ψ_- with non-equal coefficients for the two contributing MOs. For Ψ_+, the π_{Ph}* MO is expected to have the largest contribution, while for Ψ_-, π_R* is expected to have the largest coefficient. This is in agreement with TD-DFT calculations that shown that $\Psi_+ = 0.00\,\pi_{Ph}^* + 0.95\,\pi_R^*$ and $\Psi_- = 0.95\,\pi_{Ph}^* - 0.00\,\pi_R^*$. Hence, the modest lowering of the π_R* orbital energy has drastically altered the nature of the excited states, with the lowest being almost exclusively of n(pentadiene) → π*(butadiene) character (see Figure 4(c) inset). Experimentally, one would expect the photoelectron spectra to have similarities to that of Ph^- with the π_{Ph}* resonance shifted to $h\nu$ ~ 3.7 eV (as for VPh^-). We expect the transition energy to the π_{Ph}* resonance to incur small changes because there is no significant perturbation to either the π_{Ph}* orbital nor the HOMO from which the electron is excited with increased conjugation. In addition to the π_{Ph}* resonance, we expect a lower-lying state to be observable because of the lower orbital energy of π_R* in BPh^-.

Using the above framework, the frequency-resolved photoelectron spectra of $HBDI^-$, which have previously been recorded[33] and reproduced in Figure 2(d), can also be interpreted. For convenience, we ignore the methyl groups of $HDBI^-$ and only consider HBI^-. With reference to Figure 4(d), HBI^- can be viewed as phenolate conjugated via an allyl bridge to the imidazole ring. As before, there are two important π* orbitals: the phenolate π_{Ph}* orbital and the π_R*, where R is the imidazole-ring with ethene in the 2-position (Figure 4(d) inset). The Hückel energy of the π_R* orbital is $\varepsilon = \alpha - 0.35\beta$ compared to $\varepsilon = \alpha - \beta$ for π_{Ph}*. Hence, based on a comparison with BPh^-, we expect the lowest-lying exited state to be almost purely of π_R* character, while at higher energy we expect to see a resonance similar to that of Ph^-, but again shifted to $h\nu$ ~ 3.7 eV. This is broadly consistent with experimental observation. The energy gap between S_1 and the higher lying π_{Ph}*

resonance is ~1.2 eV, based on the action spectra from Andersen and coworkers.[19] The TD-DFT calculated excited states are defined by $\Psi_+ = 0.00\ \pi_{Ph}^* + 0.95\ \pi_R^*$ and $\Psi_- = 0.78\ \pi_{Ph}^* - 0.59\ \pi_R^*$. Hence, as anticipated from the BPh^-, the S_1 state is almost purely of π_R^* character. Note that the Ψ_- solution appears to have a larger than expected contribution from the π_R^* MO. This arises from excitation of HOMO–4 (the next lower-lying π_{Ph} MO) to the π_R^* MO, which is not accounted for in the current simple Hückel theory picture. Nevertheless, the dynamics of the predominantly π_{Ph}^* resonance in $HBDI^-$ are consistent with those observed for the other systems studied here. The results from our TD-DFT calculations are consistent with the high-level calculations by Bochenkova *et. al.*.[13]

The analysis for HBI^- can be compared with the Hückel interpretation of the S_1 state provided by the Krylov group.[38] They took an even more reductionist view of the S_1 state and argued that it can be viewed as a transition from the n(allyl) → π*(ethene). Although this view is elegant in its simplicity, a slight extension of this depiction provides a much more detailed and far-reaching picture. We suggest that $HBDI^-$ can be viewed as a phenolate unit and the crotonaldehyde radical (see Figure 4(d) inset). The S_1 state corresponds to a transition from the singly-occupied orbital of the crotonaldehyde radical (which has the appearance of the n(allyl) MO) to the lowest unoccupied π_R^* orbital, where R = acrolein, as shown in Figure 4(d). Hence, the S_1 is best described by n(crotonaldehyde) → π*(acrolein). The bright shape resonance identified at *hv* = 3.8 eV, S_3, corresponds a $\pi_{Ph} \rightarrow \pi_{Ph}^*$ transition localised on the phenolate and is remarkably close to the 3.7 eV that was anticipated from the simple bottom-up picture. The slight discrepancy can be attributed to the additional mixture of the HOMO–1 → π_R^* transition in the Ψ_- excited state for $HBDI^-$. The dynamics of the S_3 state have been the subject of some controversy.[13,33,36] In a previous study, we argued that the frequency resolved photoelectron spectra were most consistent with autodetachment from S_3 and internal conversion to the lower-lying dark S_2 state which subsequently autodetached.[33] However, Bochenkova *et al*. showed that the spectral broadening observed in Figure 2(d) could be reproduced as an autodetachment from the S_3 state, without invoking any internal conversion.[13] Based on the above Hückel arguments, the fact that similar spectral broadening is seen in Ph^- and $HBDI^-$ suggest that the dominant decay is simple autodetachment from the π_{Ph}^* orbital.

In principle, the above analysis is also valid for the PYP chromophore, CA^-. In fact, the Hückel structure of the relevant MOs in CA^- is essentially identical to those of HBI^-! Specifically, the same n(crotonaldehyde) → π*(acrolein) is expected to describe the S_1 state while the higher lying electronic resonances will be predominantly of π_{Ph}^* character. Hence, one may expect similar excited state structures and dynamics for the two. A study by Andersen and coworkers measured the lower lying (S_1) state of CA^- to be at an excitation energy of 2.9 eV, which is very close to the experimental electron affinity of 2.91 ± 0.05 eV,[21] as in $HBDI^-$.[14] Based on our analysis, we expect the bright resonance to lie at *hv* ~ 3.7 eV.

Relevance of Hückel picture to excited state dynamics

Although the Hückel picture is rudimentary, it provides useful insight into the basic electronic structure of bio-chromophores involving phenolates, which have been the subject of much recent interest. As the conjugation is extended further, the π_R^* MO is lowered in energy relative to the π_{Ph}^* MO, consistent with the particle in a box picture. This trivially explains why red fluorescent proteins absorb at longer wavelengths.[38] Overall, the lower the energy of the π_R^* MO is relative to that of the π_{Ph}^* MO, the more dominant its contribution to the lower-lying excited state and the lower excitation energy to the Ψ_+ excited state.

A key result here is that the VPh^- chromophore is integral to building a bottom-up understanding of biochromophores, as it represents the species in which the characteristic spectroscopic properties of photoactive proteins emerge. The mixing of the two chromophore units produces the two bright states seen in several larger bio-chromophores. In particular the excited state around *hv* = 3.7 eV has been the subject of much recent interest. The autodetachment from this resonance has been discussed in terms of photo-oxidation of GFP.[13,66] Our results show that this autodetachment process can be viewed quite simply as the loss of an electron from the lowest energy π_{Ph}^* of the phenolate (or benzene), in agreement with high-level electronic structure calculations.[13] Hence, to probe the dynamics and details of this autodetachment process, it appears not necessary to study the complex $HBDI^-$ molecule as the same dynamics can be observed in Ph^-. This is a pleasing conclusion and shows how simple chromophores of chromophores can provide exquisite insight into the dynamics of complex bio-molecules and how a gas-phase bottom-up approach can yield genuine insight into complex molecules.

One must of course recognise that the Hückel approach has major limitations and does not provide quantitative insight. Specifically, Hückel theory only predicts the nature and energies of MOs and not excited states. For excited states with character involving more than one MO, the linear combination of MOs method used here is insightful, but can only be applied to a certain extent. When excited states are combinations of many MOs, the Hückel approach fails and high-level computational methods are required. This is likely the case for higher-lying excited states. Additionally, the Hückel approach provides little information regarding the shape of excited state potential energy surfaces, although we note that bond-orders are readily calculated in Hückel theory and yield some indication of the likely initial motion away from the Franck-Condon region. Nevertheless, there is no provision for predicting dynamics, which is often one of the most important features of a chromophore's function. Finally, the protein environment also plays a deterministic role. For example, the similarity in electronic structure of the PYP and GFP chromophores does not map onto their photophysical properties or biological function; in GFP, the protein structure inhibits isomerisation which leads to the fluorescent properties of the protein, while in PYP, it does not and

isomerisation with internal conversion is the main decay mechanism. Nevertheless, we hope that the simple electronic structure and reductionist picture of photoactive protein chromophores will be useful in the development of new chromophores, particularly in synthetic laboratories that are often guided by qualitative electronic structure arguments rather than high-level *ab initio* calculations.

Conclusions

We have presented a combined frequency- and angle-resolved photoelectron and computational study of the phenolate chromophores that make up the biochromophores of photoactive proteins. A Hückel theory approach is employed to provide an understanding of the evolution of electronic structure as different para-substituents are incorporated into phenolate. For non-conjugated substituents, the electronic structure simply resembles that of bare phenolate. For conjugated substituents, a linear combination of molecular orbitals localised on the phenolate and substituent lead to the observed electronic excited states. For *p*-vinyl-phenolate, it is this effect that leads to the observation of a second bright excitation characteristic of chromophores in photoactive proteins. As the conjugation of the substituent increases, the lowering of its orbital energy defines the character of the first bright state, while the second bright state has predominantly phenolate π antibonding character. In these cases, the S_1 excited state can be described as a transition from the non-bonding orbital on the substituent including the para-carbon of phenolate to the first π antibonding orbital of the substituent excluding the para-carbon. Our results provide an intuitive and accessible framework for the logical design of photoactive chromophores.

Acknowledgements

This work was supported by the European Research Council (Starting Grant 306536). This work was conducted using the resources of the iOpenShell Center for Computational Studies of Electronic Structure and Spectroscopy of Open-Shell and Electronically Excited Species (http://iopenshell.usc.edu).

Notes and references

‡The small contribution of the second unoccupied π^* MO of phenolate is noted but this is same in all molecules and so may be expected to have the same contribution in all the anions discussed here.

1 G. H. Patterson, S. M. Knobel, W. D. Sharif, S. R. Kain and D. W. Piston, *Biophys. J.*, 1997, **73**, 2782–2790.
2 R. Y. Tsien, *Annu. Rev. Biochem.*, 1998, **67**, 509–544.
3 M. A. van der Horst and K. J. Hellingwerf, *Acc. Chem. Res.*, 2004, **37**, 13–20.
4 U. K. Genick, S. M. Soltis, P. Kuhn, I. L. Canestrelli and E. D. Getzoff, *Nature*, 1998, **392**, 206–209.
5 S. R. Meech, *Chem. Soc. Rev.*, 2009, **38**, 2922–2934.
6 M. Chattoraj, B. A. King, G. U. Bublitz and S. G. Boxer, *Proc. Natl. Acad. Sci.*, 1996, **93**, 8362–8367.
7 M. Zimmer, *Chem. Rev.*, 2002, **102**, 759–782.
8 R. F. Gunion, M. K. Gilles, M. L. Polak and W. C. Lineberger, *Int. J. Mass Spectrom. Ion Process.*, 1992, **117**, 601–620.
9 C. R. S. Mooney, D. A. Horke, A. S. Chatterley, A. Simperler, H. H. Fielding and J. R. R. Verlet, *Chem. Sci.*, 2013, **4**, 921–927.
10 1J. Tay, M. A. Parkes, K. Addison, Y. Chan, L. Zhang, H. C. Hailes, P. C. Bulman Page, S. R. Meech, L. Blancafort and H. H. Fielding, *J. Phys. Chem. Lett.*, 2017, **8**, 765–771.
11 1M. Almasian, J. Grzetic, J. Van Maurik, J. D. Steill, G. Berden, S. Ingemann, W. J. Buma and J. Oomens, *J. Phys. Chem. Lett.*, 2012, **3**, 2259–2263.
12 L. Lammich, J. Rajput and L. H. Andersen, *Phys. Rev. E*, 2008, **78**, 51916.
13 A. V. Bochenkova, C. R. S. Mooney, M. A. Parkes, J. L. Woodhouse, L. Zhang, R. Lewin, J. M. Ward, H. C. Hailes, L. H. Andersen and H. H. Fielding, *Chem. Sci.*, 2017, **8**, 3154–3163.
14 T. Rocha-Rinza, O. C. J. Rajput, A. Gopalan, D. B. Rahbek, L. H. Andersen, A. V. Bochenkova, A. A. Granovsky, K. B. Bravaya, A. V. Nemukhin, K. L. Christiansen and M. B. Nielsen, *J. Phys. Chem. A*, 2009, **113**, 9442–9449.
15 L. H. Andersen and A. V. Bochenkova, *Eur. Phys. J. D*, 2009, **51**, 5–14.
16 K. B. Bravaya and A. I. Krylov, *J. Phys. Chem. A*, 2013, **117**, 11815–11822.
17 S. Bonsma, R. Purchase, S. Jezowski, J. Gallus, F. Könz and S. Völker, *ChemPhysChem*, 2005, **6**, 838–849.
18 E. V. Gromov, I. Burghardt, H. Köppel and L. S. Cederbaum, *J. Am. Chem. Soc.*, 2007, **129**, 6798–6806.
19 A. V. Bochenkova, B. Klaerke, D. B. Rahbek, J. Rajput, Y. Toker and L. H. Andersen, *Angew. Chemie Int. Ed.*, 2014, **53**, 9797–9801.
20 J. Rajput, D. B. Rahbek, L. H. Andersen, T. Rocha-Rinza, O. Christiansen, K. B. Bravaya, A. V. Erokhin, A. V. Bochenkova, K. M. Solntsev, J. Dong, J. Kowalik, L. M. Tolbert, M. Åxman Petersen and M. Brøndsted Nielsen, *Phys. Chem. Chem. Phys.*, 2009, **11**, 9996.
21 M. A. Parkes, C. Phillips, M. J. Porter and H. H. Fielding, *Phys. Chem. Chem. Phys.*, 2016, **18**, 10329–10336.
22 C. R. S. Mooney, M. A. Parkes, A. Iskra and H. H. Fielding, *Angew. Chemie - Int. Ed.*, 2015, **54**, 5646–5649.
23 I.-R. Lee, W. Lee and A. H. Zewail, *Proc. Natl. Acad. Sci.*, 2006, **103**, 258–262.
24 L. H. Andersen, A. V. Bochenkova, J. Houmøller, H. V. Kiefer, E. Lattouf and M. H. Stockett, *Phys. Chem. Chem. Phys.*, 2016, **18**, 9909–9913.
25 P. B. Coto, D. Roca-Sanjuán, L. Serrano-Andrés, A. Martín-Pendás, S. Martí and J. Andrés, *J. Chem. Theory Comput.*, 2009, **5**, 3032–3038.
26 W. L. Ryan, D. J. Gordon and D. H. Levy, *J. Am. Chem. Soc.*, 2002, **124**, 6194–6201.
27 C. Ko, B. Levine, A. Toniolo, L. Manohar, S. Olsen, H. J. Werner and T. J. Martínez, *J. Am. Chem. Soc.*, 2003, **125**, 12710–12711.
28 S. Smolarek, A. Vdovin, D. L. Perrier, J. P. Smit, M. Drabbels and W. J. Buma, *J. Am. Chem. Soc.*, 2010, **132**, 6315–6317.
29 H. Kuramochi, S. Takeuchi and T. Tahara, *J. Phys. Chem. Lett.*, 2012, **3**, 2025–2029.
30 A. Toniolo, S. Olsen, L. Manohar and T. J. Martínez, *Faraday Discuss.*, 2004, **127**, 149–163.
31 S. B. Nielsen, A. Lapierre, J. U. Andersen, U. V. Pedersen, S. Tomita and L. H. Andersen, *Phys. Rev. Lett.*, 2001, **87**, 228102.
32 E. Kamarchik and A. I. Krylov, *J. Phys. Chem. Lett.*, 2011, **2**, 488–492.
33 C. W. West, J. N. Bull, A. S. Hudson, S. L. Cobb and J. R. R. Verlet, *J. Phys. Chem. B*, 2015, **119**, 3982–3987.

34 J. Lazzari-Dean, A. I. Krylov and K. B. Bravaya, *Int. J. Quantum Chem.*, 2015, **115**, 1258–1264.
35 A. V. Bochenkova and L. H. Andersen, *Faraday Discuss.*, 2013, **163**, 297.
36 C. R. S. Mooney, M. A. Parkes, L. Zhang, H. C. Hailes, A. Simperler, M. J. Bearpark and H. H. Fielding, *J. Chem. Phys.*, 2014, **140**, 205103.
37 A. Svendsen, H. V. Kiefer, H. B. Pedersen, A. V. Bochenkova and L. H. Andersen, *J. Am. Chem. Soc.*, 2017, jacs.7b04987.
38 K. B. Bravaya, B. L. Grigorenko, A. V. Nemukhin and A. I. Krylov, *Acc. Chem. Res.*, 2012, **45**, 265–275.
39 C. S. Anstöter, J. N. Bull and J. R. R. Verlet, *Int. Rev. Phys. Chem.*, 2016, **35**, 509–538.
40 J. Lecointre, G. M. Roberts, D. A. Horke and J. R. R. Verlet, *J. Phys. Chem. A*, 2010, **114**, 11216–24.
41 L. H. Stanley, C. S. Anstöter and J. R. R. Verlet, *Chem. Sci.*, 2017, **8**, 3054–3061.
42 W. C. Wiley and I. H. McLaren, *Rev. Sci. Instrum.*, 1955, **26**, 1150–1157.
43 A. T. J. B. Eppink and D. H. Parker, *Rev. Sci. Instrum.*, 1997, **68**, 3477–3484.
44 D. A. Horke, G. M. Roberts, J. Lecointre and J. R. R. Verlet, *Rev. Sci. Instrum.*, 2012, **83**, 63101.
45 G. M. Roberts, J. L. Nixon, J. Lecointre, E. Wrede and J. R. R. Verlet, *Rev. Sci. Instrum.*, 2009, **80**, 53104.
46 C. S. Anstöter, C. R. Dean and J. R. R. Verlet, *J. Phys. Chem. Lett.*, 2017, **8**, 2268–2273.
47 Y. Carissan, D. Hagebaum-Reignier, N. Goudard and S. Humbel, HuLiS Code: Lewis embedded in Hückel Theory.
48 Y. Carissan, D. Hagebaum-Reignier, N. Goudard and S. Humbel, *J. Phys. Chem. A*, 2008, **112**, 13256–13262.
49 Y. Shao, Z. Gan, E. Epifanovsky, A. T. B. Gilbert, M. Wormit, J. Kussmann, A. W. Lange, A. Behn, J. Deng, X. Feng, D. Ghosh, M. Goldey, P. R. Horn, L. D. Jacobson, I. Kaliman, R. Z. Khaliullin, T. Kuś, A. Landau, J. Liu, E. I. Proynov, Y. M. Rhee, R. M. Richard, M. A. Rohrdanz, R. P. Steele, E. J. Sundstrom, H. L. Woodcock, P. M. Zimmerman, D. Zuev, B. Albrecht, E. Alguire, B. Austin, G. J. O. Beran, Y. A. Bernard, E. Berquist, K. Brandhorst, K. B. Bravaya, S. T. Brown, D. Casanova, C.-M. Chang, Y. Chen, S. H. Chien, K. D. Closser, D. L. Crittenden, M. Diedenhofen, R. A. DiStasio, H. Do, A. D. Dutoi, R. G. Edgar, S. Fatehi, L. Fusti-Molnar, A. Ghysels, A. Golubeva-Zadorozhnaya, J. Gomes, M. W. D. Hanson-Heine, P. H. P. Harbach, A. W. Hauser, E. G. Hohenstein, Z. C. Holden, T.-C. Jagau, H. Ji, B. Kaduk, K. Khistyaev, J. Kim, J. Kim, R. A. King, P. Klunzinger, D. Kosenkov, T. Kowalczyk, C. M. Krauter, K. U. Lao, A. D. Laurent, K. V Lawler, S. V Levchenko, C. Y. Lin, F. Liu, E. Livshits, R. C. Lochan, A. Luenser, P. Manohar, S. F. Manzer, S.-P. Mao, N. Mardirossian, A. V Marenich, S. A. Maurer, N. J. Mayhall, E. Neuscamman, C. M. Oana, R. Olivares-Amaya, D. P. O'Neill, J. A. Parkhill, T. M. Perrine, R. Peverati, A. Prociuk, D. R. Rehn, E. Rosta, N. J. Russ, S. M. Sharada, S. Sharma, D. W. Small, A. Sodt, T. Stein, D. Stück, Y.-C. Su, A. J. W. Thom, T. Tsuchimochi, V. Vanovschi, L. Vogt, O. Vydrov, T. Wang, M. A. Watson, J. Wenzel, A. White, C. F. Williams, J. Yang, S. Yeganeh, S. R. Yost, Z.-Q. You, I. Y. Zhang, X. Zhang, Y. Zhao, B. R. Brooks, G. K. L. Chan, D. M. Chipman, C. J. Cramer, W. A. Goddard, M. S. Gordon, W. J. Hehre, A. Klamt, H. F. Schaefer, M. W. Schmidt, C. D. Sherrill, D. G. Truhlar, A. Warshel, X. Xu, A. Aspuru-Guzik, R. Baer, A. T. Bell, N. A. Besley, J.-D. Chai, A. Dreuw, B. D. Dunietz, T. R. Furlani, S. R. Gwaltney, C.-P. Hsu, Y. Jung, J. Kong, D. S. Lambrecht, W. Liang, C. Ochsenfeld, V. A. Rassolov, L. V Slipchenko, J. E. Subotnik, T. Van Voorhis, J. M. Herbert, A. I. Krylov, P. M. W. Gill and M. Head-Gordon, *Mol. Phys.*, 2015, **113**, 184–215.
50 S. Hirata and M. Head-Gordon, *Chem. Phys. Lett.*, 1999, **314**, 291–299.
51 P. J. Stephens, F. J. Devlin, C. F. Chabalowski and M. J. Frisch, *J. Phys. Chem.*, 1994, **98**, 11623–11627.
52 A. D. Becke, *J. Chem. Phys.*, 1993, **98**, 5648–5652.
53 C. Lee, W. Yang and R. G. Parr, *Phys. Rev. B*, 1988, **37**, 785–789.
54 S. H. Vosko, L. Wilk and M. Nusair, *Can. J. Phys.*, 1980, **58**, 1200–1211.
55 T. H. Dunning, *J. Chem. Phys.*, 1989, **90**, 1007–1023.
56 C. M. Oana and A. I. Krylov, *J. Chem. Phys.*, 2009, **131**, 124114.
57 C. Melania Oana and A. I. Krylov, *J. Chem. Phys.*, 2007, **127**, 234106.
58 S. Gozem and A. I. Krylov, ezDyson, http://iopenshell.usc.edu/downloads/ezdyson.
59 J. Schiedt and R. Weinkauf, *J. Chem. Phys.*, 1999, **110**, 304–314.
60 C. W. West, J. N. Bull, E. Antonkov and J. R. R. Verlet, *J. Phys. Chem. A*, 2014, **118**, 11346–11354.
61 D. A. Horke, Q. Li, L. Blancafort and J. R. R. Verlet, *Nat. Chem.*, 2013, **5**, 711–717.
62 J. N. Bull, C. W. West and J. R. R. Verlet, *Chem. Sci.*, 2015, **6**, 1578–1589.
63 D. J. Nelson, W. K. Gichuhi, E. M. Miller, J. H. Lehman and W. C. Lineberger, *J. Chem. Phys.*, 2017, **146**, 74302.
64 C. W. West, J. N. Bull, E. Antonkov and J. R. R. Verlet, *J. Phys. Chem. A*, 2014, **118**, 11346–11354.
65 T.-C. Jagau, D. B. Dao, N. S. Holtgrewe, A. I. Krylov and R. Mabbs, *J. Phys. Chem. Lett.*, 2015, **6**, 2786–2793.
66 A. Acharya, A. M. Bogdanov, B. L. Grigorenko, K. B. Bravaya, A. V. Nemukhin, K. A. Lukyanov and A. I. Krylov, *Chem. Rev.*, 2017, **117**, 758–795.

